Journal of Non-Newtonian Fluid Mechanics 196 (2013) 58–69

Contents lists available at SciVerse ScienceDirect

Journal of Non-Newtonian Fluid Mechanics

journal homepage: http://www.elsevier.com/locate/jnnfm

Absolute and convective instability of a charged viscoelastic liquid jet

Fang Li [a,b], Alfonso M. Gañán-Calvo [b,*], José M. López-Herrera [b], Xie-Yuan Yin [a], Xie-Zhen Yin [a]

[a] Department of Modern Mechanics, University of Science and Technology of China, Hefei, Anhui 230027, People's Republic of China
[b] Department of Aerospace Engineering and Fluid Mechanics, Universidad de Sevilla, Camino de los Descubrimientos s/n, 41092 Sevilla, Spain

ARTICLE INFO

Article history:
Received 17 October 2012
Received in revised form 1 January 2013
Accepted 2 January 2013
Available online 9 February 2013

Keywords:
Absolute and convective instability
Liquid jet
Electric field
Viscoelasticity

ABSTRACT

The absolute and convective instability of an electrically charged viscoelastic liquid jet is studied. The liquid is assumed to be (i) a dilute polymer solution described by the Oldroyd-B viscoelastic model, and also and (ii) a leaky dielectric defined by the Taylor–Melcher leaky dielectric theory. A generalized eigenvalue equation is obtained and solved numerically. Two different viscoelastic liquids, i.e. a PEO aqueous solution and a PIB Boger fluid, are taken as examples to study the effect of electric field and elasticity on the absolute and convective instability characteristic of the axisymmetric and first non-axisymmetric modes of a viscoelastic jet. The analysis shows that normal electric field may induce absolute instability of both axisymmetric and non-axisymmetric modes, being the effect of electric field larger on the latter. Elasticity has a profound destabilizing effect on the absolute and convective instability of the axisymmetric mode while its effect on the non-axisymmetric mode is quite limited. Strategies for suppressing absolute instability of an electrically charged viscoelastic jet are explored. The result indicates that increasing jet velocity or decreasing jet radius may effectively avoid the occurrence of absolute instability.

1. Introduction

In electrospraying and electrospinning, high-molecular polymer solutions are frequently used, see e.g. [1–4] among others. Different from Newtonian liquids, polymer solutions usually exhibit distinct rheological features. Particularly, the viscoelasticity of a polymer may substantially influence the behavior of the issued jet, consequently affecting the morphology of resulting products.

On the other hand, the behavior of a jet in either electrospraying or electrospinning is highly related to its instability characteristics. It is a well known fact that the dominant mode in electrospraying is the varicose mode, where axisymmetric perturbations tend to predominate over other perturbations, as is shown in Fig. 1a, while in electrospinning the dominant mode is the kink mode, i.e. the first non-axisymmetric perturbations are absolutely predominant ones, as is shown in Fig. 1b. These facts simply reflect the different underlying breakup mechanisms behind electrospray and electrospinning: while the object of the former process is to produce a *spray* by electrical forces, and thus breaking the jet into small pieces is essential, the latter aims to stretch a certain material (viscous liquid or polymeric solution) into extremely thin, ideally continuous filaments. In this latter case, the natural way to dramatically increase the jet's length without a drastic overall mass acceleration is to deviate and stretch the jet perpendicularly to the issuing direction, i.e. the kink mode. The force necessary to provoke this stretching perpendicular to the issuing direction of the jet is provided by the strong radial electric field generated by its own enormous surface charge.

To date, a number of researches have devoted their efforts to describe the instability of viscoelastic jets in the presence or absence of electric environments. Among them, Reneker el al. [5] and Yarin et al. [6] established a viscoelastic mode to simulate numerically the highly nonlinear bending instability of a jet in electrospinning. Brenn et al. [7] and Liu and Liu [8,9] studied the axisymmetric and non-axisymmetric instability of a non-Newtonian jet in the absence of electric fields. Carroll and Joo [10,11] studied the linear axisymmetric instability of an electrified viscoelastic jet. Montanero and Gañán-Calvo [12] analyzed the spatiotemporal instability of the axisymmetric mode of an Oldroyd-B viscoelastic liquid jet in a medium of a co-flowing liquid flow. Li et al. [13] performed a linear analysis of the competition between axisymmetric and non-axisymmetric instability of an electrically charged viscoelastic liquid jet. It was found that either the axisymmetric mode or the first non-axisymmetric mode is predominant in jet instability depending on the level of electrification and that elasticity destabilizes both modes, particularly the axisymmetric one. Ruo et al. [14] examined the influence of unrelaxed elastic tension on the three-dimensional temporal instability of a viscoelastic liquid jet. They concluded that in the presence of unrelaxed tension elasticity plays a stabilizing role in the instability of the axisymmetric and

* Corresponding author. Tel.: +34 954 487226; fax: +34 954 486041.
E-mail addresses: fli6@ustc.edu.cn (F. Li), amgc@us.es (A.M. Gañán-Calvo), jmlopez@us.es (J.M. López-Herrera).

0377-0257/$ - see front matter © 2013 Elsevier B.V. All rights reserved.
http://dx.doi.org/10.1016/j.jnnfm.2013.01.003

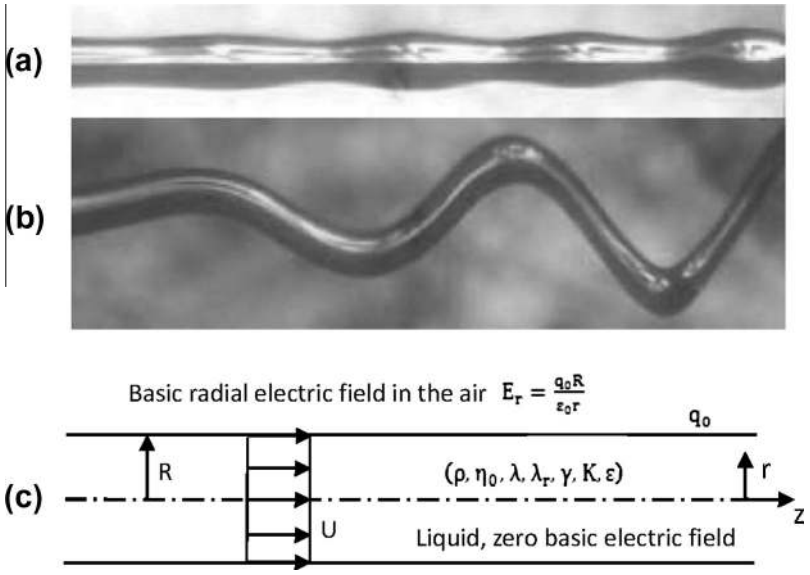

Fig. 1. Photographs of (a) the axisymmetric varicose mode, (b) the non-axisymmetric kink mode, and (c) schematic description of the theoretical model.

non-axisymmetric modes. Later they extended their research to the electric environment [15].

Electric field is the driving factor in electrospraying and electrospinning. First, at the outlet of flow, electric field provides the conditions for the formation of a critically stable meniscus structure, which is called Taylor cone, characterized by the equilibrium between surface tension and the electrostatic force due to the surface charges. In turn, this meniscus provides the sustaining mechanic structure for a singular fluidic phenomenon: from its apex, a stable, extremely thin jet is formed under certain electric potential and flow rate. The diameter of that jet is normally two or three orders smaller than that of the outlet, down to micro-and nano-meters [16–18]. The downstream evolution and breakup of the electrically charged jet yields small drops and ultra-fine fibers. The electric field due to the surface charges promotes the instability of jet, enhancing its breakup into droplets or its violent stretching by a whipping movement [13,19]. Besides, the electric charges induced by the electric field in the droplets and fibers normally prevent their coalescence before solidification takes place [20].

The present work is motivated by the fact that in electrospraying and electrospinning the stable cone-jet structure is only formed under a certain range of applied electric fields and flow rates. Beyond this range the jet may become globally unstable, which may provoke catastrophic situations in continuous production [21–23]. Therefore it is of importance to study the global instability of the jet. Here, the absolute-convective instability transition provided by a spatiotemporal analysis is the first step to understand the global instability phenomenon [24–29]. Absolute and convective instability was soon identified as a fundamental concept in instability analysis. In fact, while convective instabilities leave the system locally unaffected (they are "flushed" by the basic flow), absolute instabilities grow without limitation at the point where they appear, leading to a global catastrophe of the system. In practical terms, for a flow released from a capillary, if a jet is formed and becomes unstable at some distance downstream, it is regarded to be convectively unstable, but if no jet is formed and instability happens near the exit of capillary, the hypothetical jet structure is regarded to be absolutely unstable [30].

The absolute and convective instability of jet has been studied extensively. Taking an axisymmetric model of a charged Newtonian liquid jet, López-Herrera et al. [24] calculated the critical Weber number at the boundary of absolute and convective instability and found that the electric force has a secondary role in the absolute to convective instability transition of jet. Extending their research to three-dimensional scope, Li et al. [25] studied systematically the linear spatiotemporal instability of a viscous jet of low permittivity, low conductivity liquid under both radial and axial electric fields. The absolute and convective instability transition was explored in the four-parameter space (the Weber number, the Reynolds number, the electrical Bond number and the tangential electric field) for both the axisymmetric and first non-axisymmetric modes. Taking flow focusing as application background, Herrada et al. [26] studied the jetting-dripping transition of a compound capillary jet. They calculated the critical Weber number as a function of the radius ratio for the axisymmetric case. Vega et al. [27] studied experimentally and numerically the influence of the flow rate, the distance between the capillary meniscus and the orifice, as well as liquid properties on the status of flow. Three different regimes, i.e. the steady jetting regime, the local instability regime and the global instability regime, were identified. Montanero et al. [28] and Acero et al. [29] performed an experimental study on the global instability of a viscous liquid jet focused by a coaxial jet stream, considering different geometric configurations of the experimental apparatus utilized to generate the jet. Si et al. [31] explored the modes in flow focusing, among which the axisymmetric jetting mode was considered to be convectively unstable and the dripping mode to be absolutely unstable. Clasen et al. [32] investigated the jetting-dripping transition of a dilute polymer solution jet.

In this paper we investigate the absolute and convective instability of an electrified viscoelastic liquid jet. It is organized as follows. In Section 2 the theoretical model is established and the formulation is presented. The governing equations and boundary conditions are transformed into a generalized eigenvalue problem and the numerical method utilized to solve the problem is briefly stated. In Section 3 the absolute and convective instability characteristic of the axisymmetric and first non-axisymmetric modes of the selected liquid jets are explored. The effects of normal electric field and elasticity on the absolute and convective instability of the unstable modes are studied. In addition, strategies for suppressing absolute instability of a viscoelastic jet are discussed. In Section 4 main conclusion is drawn.

As a general consideration, this work aims to provide additional theoretical basis for the adequate physical description of

electrospinning phenomena, like other published works in the literature on this subject. Owing to the current imperfect understanding of these phenomena, many published experimental works provide limited and incomplete description of results: indeed, their comparison with theoretical models leads to an end point because the absence of reporting on critical or crucial experimental observations precludes building a complete description. This study aims to dissect some illustrating cases within the appropriate physical space of parameters that describe and qualify electrospinning phenomena in the framework of the assumptions made.

2. Model and formulation

2.1. Theoretical model and linearized equations

The present theoretical model shares many characteristics with the one established in our previous study [13]. We consider an infinitely long cylindrical liquid jet of radius R, surrounded by stationary air or vacuum (negligible dynamical effect), see Fig. 1c. The basic velocity of the jet is steady and uniform, and only has nonzero axial component, which is denoted by U. The liquid is supposed to be incompressible and viscoelastic. Its viscoelasticity is described by the Oldroyd-B constitutive equation [33]. It is also supposed to be a Taylor–Melcher leaky dielectric of finite electrical conductivity K and electrical permittivity ε [34]. The electrical permittivity of surrounding air or vacuum is ε_0.

The dominant slenderness of the jet and the leaky dielectric nature of the liquid [34] used in these phenomena brings on an electric field configuration where the normal electric field on the jet surface is much larger than the tangential one. Thus, the jet slenderness provides that the radial electric field is much larger than the axial one. In order to carry out a theoretically instability analysis, here we neglect the axial electric field, assuming that a free charge of density q_0 is present on the surface of a cylindrical jet. As a result a basic radial electric field $q_0R/\varepsilon_0 r$ is formed in the air medium, where r is the radial coordinate in the cylindrical coordinate system (r,θ,z) with θ and z the azimuthal and axial coordinates, respectively. Consistently with the underestimation of the axial electric field, no basic electric field in the liquid bulk is considered. When the jet is perturbed, the electrical relaxation time is assumed small enough to allow the relaxation of all charges on the surface. The absence of bulk charges is thus consistent with the absence of electric field in the bulk. Actually, in our simplified model electric stresses only exist on jet surface. In addition, the effects of the gravitational force, temperature and magnetic field are assumed to be negligible.

Suppose the jet is perturbed by an infinitesimal disturbance. The linearized continuity equation and momentum equation in nondimensional form are

$$\nabla \cdot \boldsymbol{v} = 0, \tag{1}$$

and

$$\left(\frac{\partial}{\partial t} + \frac{\partial}{\partial z}\right)\boldsymbol{v} = -\nabla p + \nabla \cdot \boldsymbol{\tau}, \tag{2}$$

where $\boldsymbol{v}$ is the velocity perturbation, t is the time, p is the pressure perturbation and $\boldsymbol{\tau}$ is the stress tensor. According to the Oldroyd-B viscoelastic model, the relationship between stress and strain is

$$\left[1 + D_e\left(\frac{\partial}{\partial t} + \frac{\partial}{\partial z}\right)\right]\boldsymbol{\tau} = \frac{2}{R_e}\left[1 + \lambda^*\left(\frac{\partial}{\partial t} + \frac{\partial}{\partial z}\right)\right]\boldsymbol{D}, \tag{3}$$

where $\boldsymbol{D}\left(=\frac{1}{2}[\nabla\boldsymbol{v} + (\nabla\boldsymbol{v})^T]\right)$ is the strain rate tensor. Three dimensionless numbers appear in Eq. (3), i.e. the Deborah number $D_e = \lambda U/R$ with λ the stress relaxation time, the Reynolds number $R_e = \rho UR/\eta_0$ with ρ the liquid density and η_0 the zero-shear viscosity, and the relative retardation time $\lambda^* = \lambda_r U/R$ with λ_r the strain retardation time.

The governing Laplace equation for the electric potential

$$\nabla^2 \varphi_{,a} = 0, \tag{4}$$

closes the governing equations, where φ represents the potential in the liquid phase, φ_a represents the potential in the air phase, and the electric field intensity is $\boldsymbol{E}_{,a} = -\nabla\varphi_{,a}$.

The linearized boundary conditions at the interface of the liquid jet and the ambient medium, whose position is $r = 1 + f$, are summarized below.

(i) The kinematic boundary condition

$$v = \left(\frac{\partial}{\partial t} + \frac{\partial}{\partial z}\right)f, \tag{5}$$

where v is the velocity component in radial direction and f is the small displacement of the interface deviated from its equilibrium position.

(ii) The dynamic boundary condition

$$\|\boldsymbol{T}\| \cdot \boldsymbol{n} - \frac{1}{W_e}\nabla \cdot \boldsymbol{n}\boldsymbol{n} = 0, \tag{6}$$

where $\boldsymbol{n}$ is the normal unit vector and $\nabla \cdot \boldsymbol{n}$ is the surface curvature. The stress tensor $\boldsymbol{T}$ comprises the hydrodynamic stress $\boldsymbol{T}^h$ $(= -p\boldsymbol{\delta} + \boldsymbol{\tau}^h$, where $\boldsymbol{\delta}$ is the identity matrix and $\boldsymbol{\tau}^h$ is the viscous stress) and the electrical stress $\boldsymbol{T}^e$. For the liquid phase $\boldsymbol{T}^e = \varepsilon_r E_u\left(\boldsymbol{E}\boldsymbol{E} - \frac{1}{2}\boldsymbol{E}\cdot\boldsymbol{E}\boldsymbol{\delta}\right)$ and for the air phase $\boldsymbol{T}^e = E_u\left(\boldsymbol{E}_a\boldsymbol{E}_a - \frac{1}{2}\boldsymbol{E}_a\cdot\boldsymbol{E}_a\boldsymbol{\delta}\right)$. Three dimensionless numbers appear in Eq. (6), i.e. the Weber number $W_e = \rho U^2 R/\gamma$ with γ the surface tension coefficient, the relative electrical permittivity $\varepsilon_r = \varepsilon/\varepsilon_0$ and the electrical Euler number $E_u = q_0^2/\varepsilon_0\rho U^2$.

(iii) The electric field satisfies the continuity of tangential electric field and the Gauss law at surface, i.e.

$$\boldsymbol{n} \times (\boldsymbol{E}_a - \boldsymbol{E}) = 0, \tag{7}$$

$$(\boldsymbol{E}_a - \varepsilon_r\boldsymbol{E}) \cdot \boldsymbol{n} = q, \tag{8}$$

where q is the surface charge density satisfying the following conservation equation

$$\left(\frac{\partial}{\partial t} + \frac{\partial}{\partial z}\right)q - \frac{\partial v}{\partial r} - \tau_e\varepsilon_r\boldsymbol{E}\cdot\boldsymbol{n} = 0, \tag{9}$$

where $\tau_e = KR/\varepsilon U$ is the relative electrical relaxation time of the jet.

2.2. Equations for absolute and convective instability analysis

In spatiotemporal instability analysis the relevant variables of a system are supposed to be perturbed by an arbitrary infinitesimal three-dimensional disturbance of the form $A(r)\exp[i(kz + m\theta) - i\omega t]$ (normal mode analysis), where the prefactor $A(r)$ is the eigenfunction of any specific variable (velocity, pressure or electric field), i is the imaginary number, k is the complex axial wave number, m is the azimuthal wave number (integer) and ω is the complex frequency. Substituting the normal mode disturbance into the governing equations and boundary conditions (1)–(9), a series of linear homogeneous equations of the eigenfunctions is obtained.

The continuity Eq. (1) and the momentum Eq. (2) yield

$$\frac{d\hat{v}}{dr} + \frac{\hat{v}}{r} + \frac{im}{r}\hat{w} + ik\hat{u} = 0, \tag{10}$$

$$(-i\omega + ik)\hat{v} = -\frac{d\hat{p}}{dr} + \eta\left[\frac{d^2\hat{v}}{dr^2} + \frac{1}{r}\frac{d\hat{v}}{dr} - \left(\frac{m^2+1}{r^2} + k^2\right)\hat{v} - \frac{2im}{r^2}\hat{w}\right], \tag{11}$$

$$(-i\omega+ik)\hat{w}=-\frac{im}{r}\hat{p}+\eta\left[\frac{d^2\hat{w}}{dr^2}+\frac{1}{r}\frac{d\hat{w}}{dr}-\left(\frac{m^2+1}{r^2}+k^2\right)\hat{w}+\frac{2im}{r^2}\hat{v}\right], \tag{12}$$

$$(-i\omega+ik)\hat{u}=-ik\hat{p}+\eta\left[\frac{d^2\hat{u}}{dr^2}+\frac{1}{r}\frac{d\hat{u}}{dr}-\left(\frac{m^2}{r^2}+k^2\right)\hat{u}\right], \tag{13}$$

where w and u are the velocity components in azimuthal and axial directions, respectively, the cap denotes the eigenfunction of the corresponding perturbed variable, and η is a compound parameter expressed as

$$\eta=\frac{1}{R_e}\frac{1-i\lambda^*(\omega-k)}{1-iD_e(\omega-k)}.$$

The kinematic boundary condition (5) yields

$$\hat{v}=-i(\omega-k)\hat{f}. \tag{14}$$

Owing to the decoupling of the electric field with the flow field in liquid bulk, the electric field can be solved individually. From Eq. (4) the eigenfunction of electric potential perturbation $\hat{\varphi}_{,a}$ satisfies the modified Bessel equation

$$\frac{d^2\hat{\varphi}_{,a}}{dr^2}+\frac{1}{r}\frac{d\hat{\varphi}_{,a}}{dr}-(k^2+\frac{m^2}{r^2})\hat{\varphi}_{,a}=0.$$

Considering the finiteness at the symmetry axis $r=0$ and the far field $r\to\infty$, the solutions to the above equation are

$$\hat{\varphi}=C_1I_m(kr)\ \text{and}\ \hat{\varphi}_a=C_2K_m(kr),$$

where $I_m(k)$ and $K_m(k)$ are the m^{th} modified Bessel functions of the first and second kinds, respectively, and C_1 and C_2 are the coefficients to be determined by boundary conditions. Hence the perturbation of electric field intensity is

$$\boldsymbol{E}=\left[-C_1kI'_m(kr),-\frac{im}{r}C_1I_m(kr),-ikC_1I_m(kr)\right]\exp[i(kz+m\theta)-i\omega t],$$

$$\boldsymbol{E}_a=\left[-C_2kK'_m(kr),-\frac{im}{r}C_2K_m(kr),-ikC_2K_m(kr)\right]\exp[i(kz+m\theta)-i\omega t],$$

where the prime denotes the first derivative with respect to argument. Substituting the expressions into the boundary conditions (7) and (8), we get

$$C_1=\frac{\hat{q}+\hat{f}\xi}{kI'_m(k)\zeta}\ \text{and}\ C_2=\frac{C_1I_m(k)+\hat{f}}{K_m(k)},$$

where

$$\xi=1+k\frac{K'_m(k)}{K_m(k)},\quad \zeta=\varepsilon_r-\frac{I_m(k)K'_m(k)}{I'_m(k)K_m(k)}.$$

Substituting the solutions of electric field into the dynamic boundary condition (6) and the surface charge conservation Eq. (9) yields

$$\hat{p}-2\eta\frac{d\hat{v}}{dr}+E_u\left(1-\frac{\varepsilon_r}{\zeta}\right)\hat{q}+\left(\frac{1-m^2-k^2}{W_e}-E_u\frac{\varepsilon_r\xi}{\zeta}\right)\hat{f}=0, \tag{15}$$

$$\eta\left(im\hat{v}+\frac{d\hat{w}}{dr}-\hat{w}\right)+\frac{imE_u}{k\zeta}\frac{I_m(k)}{I'_m(k)}\hat{q}+\frac{imE_u\xi}{k\zeta}\frac{I_m(k)}{I'_m(k)}\hat{f}=0, \tag{16}$$

$$\eta\left(\frac{d\hat{u}}{dr}+ik\hat{v}\right)+\frac{iE_u}{\zeta}\frac{I_m(k)}{I'_m(k)}\hat{q}+\frac{iE_u\xi}{\zeta}\frac{I_m(k)}{I'_m(k)}\hat{f}=0, \tag{17}$$

$$\left(-i\omega+ik+\frac{\tau_e\varepsilon_r}{\zeta}\right)\hat{q}-\frac{d\hat{v}}{dr}+\frac{\tau_e\varepsilon_r\xi}{\zeta}\hat{f}=0. \tag{18}$$

The bulk Eqs. (10)–(13) together with the boundary conditions (14)–(18) constitute the generalized eigenvalue equation system of this problem.

2.3. Numerical method

The problem is solved numerically by means of Chebyshev spectral collocation method. First, the physical space $r\in[0,1]$ is transformed into the calculation space $y\in[-1,1]$. Considering the basic velocity profile of the jet is uniform, a simple linear transformation is appropriate, i.e.

$$r=\frac{1+y}{2}.$$

Consistency conditions need to be imposed on the symmetry axis $r=0$ to eliminate the singularity, i.e.

$$\begin{aligned}&\hat{v}=\hat{w}=\frac{d\hat{u}}{dr}=\frac{d\hat{p}}{dr}=0\ \text{for}\ m=0,\\ &\hat{u}=\hat{p}=0,\quad \hat{v}+i\hat{w}=0,\quad 2\frac{d\hat{v}}{dr}+i\frac{d\hat{w}}{dr}=0\ \text{for}\ m=1,\\ &\hat{v}=\hat{w}=\hat{u}=\hat{p}=0\ \text{for}\ m>1.\end{aligned} \tag{19}$$

In the domain $y\in[-1,1]$ the bulk eigenfunctions $\hat{v},\hat{w},\hat{u}$ and $\hat{p}$ are expanded as a sum of Chebyshev polynomials, i.e.

$$\hat{v}(y)=\sum_{n=0}^{N}a_nT_n(y),$$

$$\hat{w}(y)=\sum_{n=0}^{N}b_nT_n(y),$$

$$\hat{u}(y)=\sum_{n=0}^{N}c_nT_n(y),$$

$$\hat{p}(y)=\sum_{n=0}^{N}d_nT_n(y),$$

where $T_n(y)=\cos[n\cos^{-1}(y)]$ is the Chebyshev polynomial, a_n, b_n, c_n and d_n are the expansion coefficients and N is the number of the polynomials. The continuity Eq. (10) and the momentum Eqs. (11)–(13) are evaluated at the Gauss–Lobatto collocation points $y_j=\cos(j\pi/N)$, $j=0,1,\ldots,N$. In the calculation 20–30 collocation points are sufficient to ensure the convergence. The boundary conditions are also evaluated at the corresponding points. The dynamic boundary conditions (15)–(17) replace the momentum equations at the jet surface $r=1+f$. The consistency conditions (19) replace the continuity equation and the momentum equations at the symmetric axis $r=0$. Note that the momentum equations are quadratic equations of ω. The eigenvalue equation can be written in the following form

$$\omega^2[D]\boldsymbol{Y}+\omega[C]\boldsymbol{Y}=[B]\boldsymbol{Y}, \tag{20}$$

where the vector $\boldsymbol{Y}=[a_0,\cdots,a_n,b_0,\cdots,b_n,c_0,\cdots,c_n,d_0,\cdots,d_n,\hat{q},\hat{f}]^T$ and $[B]$, $[C]$ and $[D]$ are the coefficient matrices of size $(4N+6)\times(4N+6)$. The expressions of $[B]$, $[C]$ and $[D]$ are given in Appendix A. To solve the problem, the above equation should be transformed into a generalized eigenvalue problem as follows [14,15]

$$[E]\boldsymbol{X}=\omega[F]\boldsymbol{X}, \tag{21}$$

where

$$\boldsymbol{X}=\begin{pmatrix}\boldsymbol{Y}\\ \omega\boldsymbol{Y}\end{pmatrix},\quad [E]=\begin{bmatrix}B & 0\\ 0 & I\end{bmatrix},\quad [F]=\begin{bmatrix}C & D\\ I & 0\end{bmatrix},$$

and I is the unit matrix of size $(4N+6)\times(4N+6)$. The generalized eigenvalue problem (20) is solved using a Matlab code.

Due to the uniformity of the basic velocity profile, a dispersion relation can be derived, which is basically the same as in our previous paper [13] if ω is replaced with $-i\omega$. The dispersion relation is solved with the aid of Muller's method in ISML, serving as a check to the validity of the Matlab code.

3. Result and discussion

In this section the absolute and convective instability of the axisymmetric mode $m = 0$ and the first non-axisymmetric mode $m = 1$ of a charged viscoelastic jet is studied. For each mode, the complex frequency ω is solved as function of the axial wave number k and the dimensionless parameter set $(R_e, D_e, \lambda^*, W_e, \tau_e, \varepsilon_r, E_u)$. Due to the complexity of the problem, two particular viscoelastic liquids, i.e. a PEO aqueous solution and a PIB Boger fluid, are chosen as samples, as performed in our previous paper [13]. PEO aqueous solutions and PIB Boger fluids are simple viscoelastic experimental materials frequently used in electrospraying and electrospinning. They have distinct differences in viscosity, elasticity, surface tension and electrical properties, which may lead to different jet instability behaviors. The choice of both liquids and the theoretical viscoelastic model is dictated by a further comparison with experiments: both PEO aqueous solutions and PIB Boger fluids are dilute polymer solutions well described by the Oldroyd-B viscoelastic constitutive equation. Their physical properties were given in [10,13]. Fixing the radius of jet to 10 μm and the velocity of jet to 1 m/s, a reference state is established, as shown in Table 1. The values of the dimensionless parameters are kept under the reference state unless otherwise stated.

The typical contour plots of the imaginary part of the complex frequency ω_i in the complex wave number k plane for the axisymmetric and non-axisymmetric modes of the PEO aqueous solution and the PIB Boger fluid are shown in Figs. 2 and 3, for, respectively. Evidently there is a saddle point in each plot. In Fig. 2a the location of the saddle point is $k_0 = (1.15, -0.19)$ and the value of the complex frequency at the saddle point is $\omega_0 = (1.12, 1.18)$; in Fig. 2b $k_0 = (0.62, -0.21)$, $\omega_0 = (0.60, 0.96)$; in Fig. 3a $k_0 = (1.30, -2.25)$, $\omega_0 = (1.44, -1.47)$; and in Fig. 3b $k_0 = (0.55, -0.15)$, $\omega_0 = (0.56, 1.18)$. All the saddles satisfy the Briggs pinching criterion [35]. Normally, k_0 is referred to as the absolute wave number and ω_0 the absolute frequency. The absolute and convective instability characteristic of a jet is determined by the imaginary part of the absolute frequency, i.e. the absolute growth rate ω_{0i}. In Fig. 2a and b the absolute growth rate is positive, indicating that both the axisymmetric and non-axisymmetric modes of the PEO aqueous solution are absolutely unstable. In Fig. 3a it is negative, indicating that the axisymmetric mode of the PIB Boger fluid is convectively unstable, whereas the non-axisymmetric mode of the fluid is absolutely unstable with a positive absolute growth rate, as shown in Fig. 3b.

3.1. Effect of electric field on absolute and convective instability of jet

The effect of the normal electric field on the absolute and convective instability of jet of the PEO aqueous solution and the PIB Boger fluid is illustrated in Fig. 4, where squares and circles denote data points and solid and dashed lines denote fitting curves. It can be seen in the figure that the axisymmetric mode of the PEO aqueous solution is absolutely unstable, even in the absence of electric field (i.e. $E_u = 0$). As the electric field increases, the absolute instability of the axisymmetric mode is strengthened. The non-axisymmetric mode of the PEO aqueous solution was already known to be temporally stable in the absence of electric field, but it can be made unstable by an imposed electric field [13]. Such a fundamental influence of electric field on the non-axisymmetric mode is also shown in Fig. 4. When electric field is absent, the absolute growth rate of the non-axisymmetric mode is negative. When the electrical Euler number is increased to a small value ($E_u \approx 2$), it becomes positive. That is, only within a narrow range of the electrical Euler number (about $0 < E_u < 2$) the non-axisymmetric mode is convectively unstable. Beyond this range it is absolutely unstable. In addition, electric field has a more profound effect on the non-axisymmetric mode than on the axisymmetric mode. At sufficiently large electric fields the absolute growth rates of them are comparable.

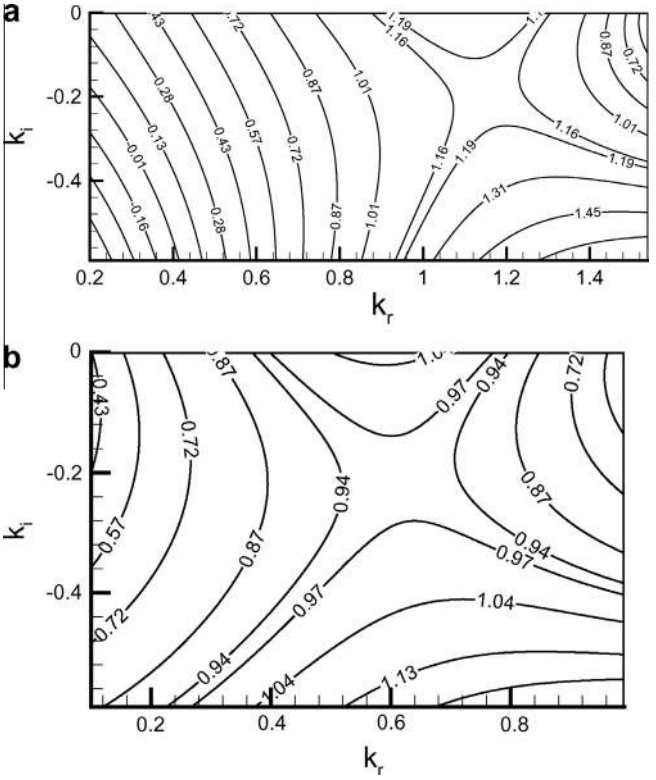

Fig. 2. Contours of the imaginary part of the complex frequency ω_i in the complex wave number plane for (a) the axisymmetric mode $m = 0$ and (b) the non-axisymmetric mode $m = 1$ of the PEO aqueous solution.

Different from the PEO aqueous solution, the behavior of the axisymmetric mode of the PIB Boger fluid is quite peculiar. Although the absolute growth rate of it is increased by electric field to a certain extent, the mode remains convectively unstable in the calculation range $E_u \in [0, 20]$. Nevertheless, the tendency suggests that it may become absolutely unstable at larger electric field. On the other hand, the non-axisymmetric mode is stable at zero electric field. As the electric field increases, the mode first becomes convectively unstable and soon enters the absolute instability region at an even smaller electrical Euler number than that of the non-axisymmetric mode of the PEO aqueous solution. After it becomes absolutely unstable the electric field continuously increases its absolute growth rate. Compared with the axisymmetric mode, apparently the non-axisymmetric mode is much more unstable in most situations. That is, the non-axisymmetric mode dominates over the axisymmetric mode in the stability of jet of the PIB Boger

Table 1
Values of the dimensionless parameters under the reference state.

	R_e	D_e	λ^*	W_e	τ_e	ε_r	E_u
PEO-2M	0.01	2.0×10^4	20	0.1471	197.74	80	10
PIB Boger fluid 4000 ppm	0.0833	311	146.48	0.5822	0.0113	3	10

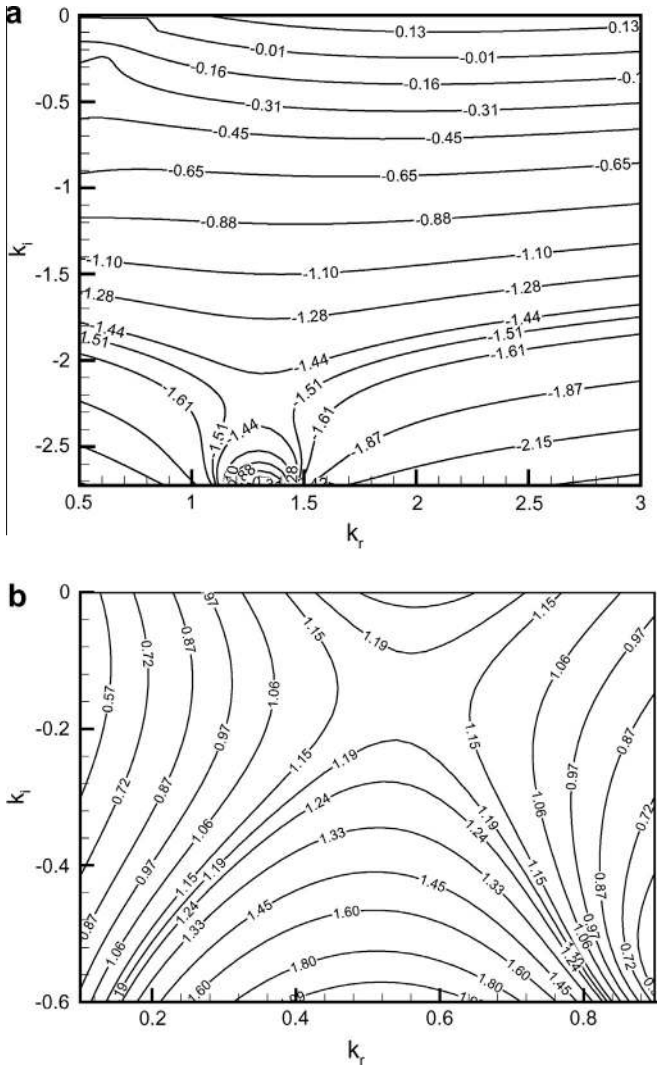

Fig. 3. Contours of the imaginary part of the complex frequency ω_i in the complex wave number plane for (a) the axisymmetric mode $m = 0$ and (b) the non-axisymmetric mode $m = 1$ of the PIB Boger fluid.

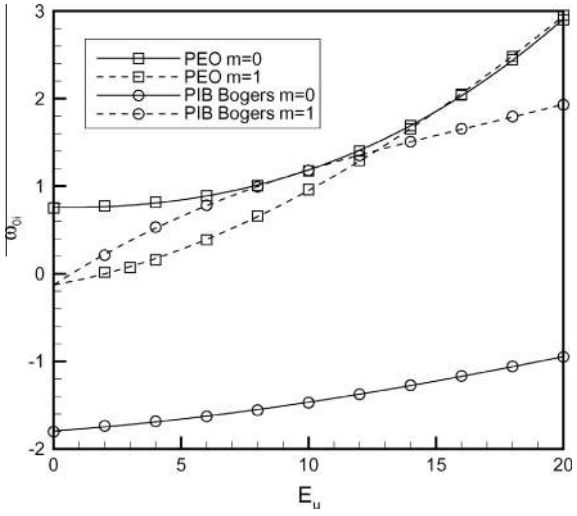

Fig. 4. The absolute growth rate ω_{0i} versus the electrical Euler number E_u.

fluid. The same conclusion was drawn from the temporal instability study [13].

Recently Si et al. [21] performed an experimental investigation on the flow modes in electrospinning using aqueous PEO solutions. It was found that when the electric potential exceeds a certain critical value the stable bending mode cannot be maintained and several irregular modes appear. These irregular modes may be the result of a global instability caused by the absolute instability under a large applied electric field. From this point, our theoretical prediction above is qualitatively in agreement with the experiments.

3.2. Effect of elasticity on absolute and convective instability of jet

There are two dimensionless parameters related to liquid elasticity, i.e. the Deborah number D_e and the relative strain retardation time λ^*. It is understood that the Deborah number is of much more significance in the instability of a viscoelastic jet [9]. Hence we study the effect of elasticity on the absolute and convective instability of jet only through this parameter. In practice, changing elasticity usually implies a modification of the other physical properties of liquid, but we disregard this fact and assume that the Deborah number can be adjusted freely while maintaining the other parameters unchanged.

Figs. 5a and 5b illustrate the absolute growth rate ω_{0i} of the axisymmetric mode and the non-axisymmetric mode of jet of the PEO aqueous solution, respectively, versus the electrical Euler number E_u, for different values of the Deborah number. As is shown in Fig. 5a, when the elasticity of liquid is small (e.g. $D_e = 200$), the axisymmetric mode is convectively unstable and the effect of electric field is quite small. When the elasticity of liquid is sufficiently large, the axisymmetric mode becomes absolutely unstable. As elasticity increases, the absolute instability of the mode is further enhanced. The destabilization effect of elasticity on the axisymmetric mode is more significant at large electric fields. Contrarily, the effect of elasticity on the non-axisymmetric mode is weak. As is shown in Fig. 5b, at relatively small electric fields the non-axisymmetric mode is hardly influenced by elasticity and at relatively large electric fields it is destabilized by elasticity to a small extent.

Figs. 6a and 6b illustrate the result for the PIB Boger fluid. Clearly elasticity weakens the convective instability of the axisymmetric mode of the fluid. Moreover, at sufficiently large electric fields the axisymmetric mode may become absolutely unstable. On the other hand, the destabilization effect of elasticity on the non-axisymmetric mode is limited, as in the case of the PEO aqueous solution.

3.3. Strategies for suppressing absolute instability

Normally, absolute instability is undesirable in electrospraying and electrospinning since it potentially induces the global instability of jet and influences the quality of products. Unfortunately, our calculation result shows that the axisymmetric mode of a viscoelastic jet is probably absolutely unstable if the elasticity of liquid and the imposed normal electric field are large enough. More surprisingly, the non-axisymmetric mode becomes absolutely unstable easily once its instability is triggered, no matter how large the elasticity is. From this perspective, it is of interest to seek for some strategy for suppressing absolute instability of a charged viscoelastic jet.

In addition to the Deborah number and the electrical Euler number, the Reynolds number and the Weber number are naturally supposed to be two parameters influencing the absolute and convective instability characteristic of jet. However, according to our calculation, absolute instability cannot be completely suppressed by varying the Reynolds number or the Weber number individually, even though they show great quantitative influence on jet instability. For the PEO aqueous solution, within the range

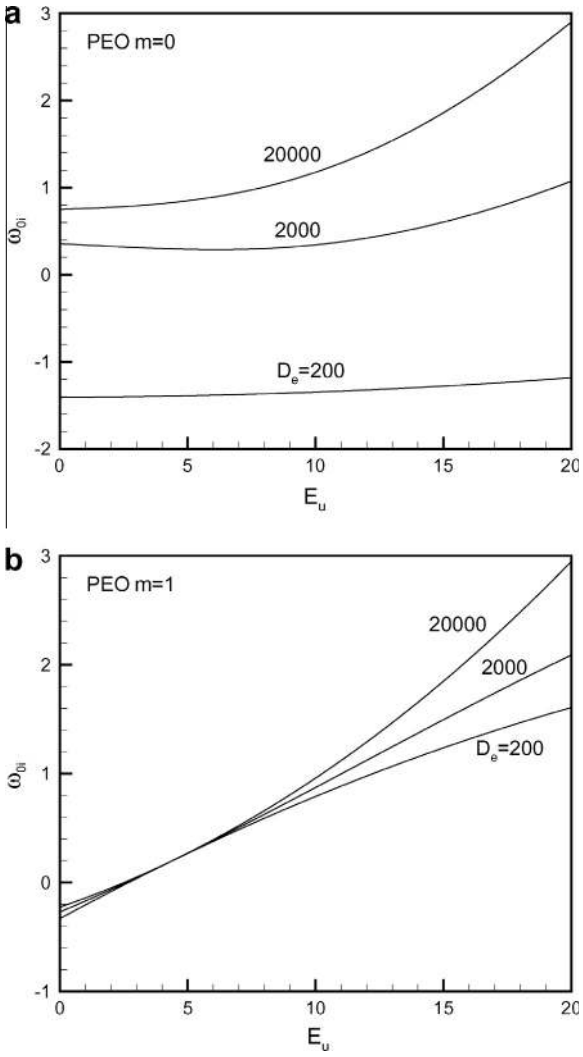

Fig. 5. Effect of the elasticity on the absolute and convective instability of (a) the axisymmetric mode $m = 0$ and (b) the non-axisymmetric mode $m = 1$ of the PEO aqueous solution.

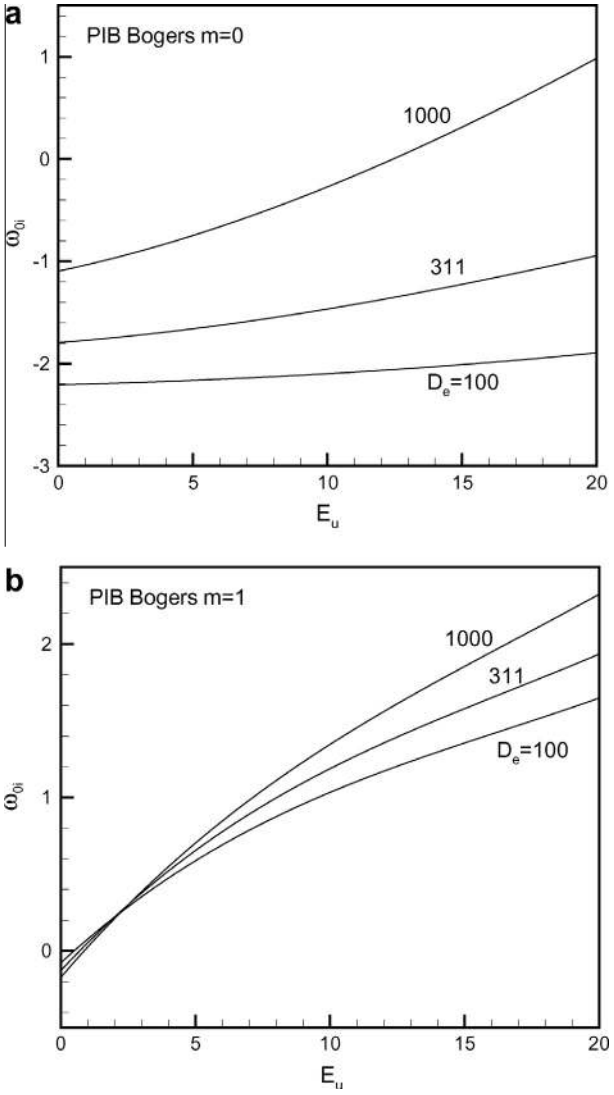

Fig. 6. Effect of the elasticity on the absolute and convective instability of (a) the axisymmetric mode $m = 0$ and (b) the non-axisymmetric mode $m = 1$ of the PIB Boger fluid.

from 0.001 to 0.1 the Reynolds number increases the absolute growth rate of both the axisymmetric and non-axisymmetric modes. Absolute instability cannot be avoided even at extremely small Reynolds number ($R_e = 0.001$). For the PIB Boger fluid, the Reynolds number also destabilizes the axisymmetric and non-axisymmetric modes within the range $R_e \in [0.01, 0.5]$. The axisymmetric mode becomes absolutely unstable at large values of the Reynolds number and large electric fields, while the non-axisymmetric mode is absolutely unstable all the way. The influence of the Weber number on the axisymmetric and non-axisymmetric modes for the PEO aqueous solution is complicated, but both modes are basically kept in the absolute instability domain within the range $W_e \in [0.05, 0.3]$. As to the PIB Boger fluid, for $W_e \in [0.1, 10]$ the axisymmetric mode remains convectively unstable, being the absolute growth rate increased as the Weber number decreases. On the other hand, the non-axisymmetric mode is always absolutely unstable, even though its absolute growth rate is depressed greatly at small values of Weber number. Generally, for neither the PEO aqueous solution nor the PIB Boger fluid it seems feasible to eliminate absolute instability through changing viscosity or surface tension of liquid. We need to explore other aspects.

In the calculation the velocity and the radius of jet are fixed for convenience. However, in experiments both the velocity and the radius of jet can be changed through adjusting the flow rate at the orifice of capillary. Considering this fact, in the following we study the effect of them on the absolute and convective instability of jet, aiming to find possible ways to suppress absolute instability.

First, the radius of jet is fixed to 10 μm and the velocity of jet is varied between several values: 0.5 m/s, 1 m/s, 2 m/s and 4 m/s. Note that with the variation of the velocity of jet six parameters, i.e. R_e, D_e, λ^*, W_e, τ_e and E_u, are changed at the same time. In such a case the electrical Euler number is not appropriate as abscissa in the plot and we use the nondimensional electrostatic pressure $\varpi = q_0^2\eta_0^2/\varepsilon_0\rho\gamma^2$ instead. Here, note that the value of ϖ is about two orders larger than the value of the electrical Euler number. In this sense the characteristic pressure $\rho\gamma^2/\eta_0^2$ would not be appropriate as a scale to normalize the electrostatic force. However, it does not affect our analysis. In addition, the velocity of jet is scaled by $U_c = \gamma/\eta_0$, that is, the nondimensional velocity of jet is defined as $U^* = U/U_c$. Figs. 7a and 7b illustrate the variation of the absolute growth rate with the nondimensional velocity of jet for the axisymmetric mode and the non-axisymmetric mode of the PEO aqueous solution, respectively. It is clear that absolute instability of both modes is suppressed as the velocity of the jet is increased. At a velocity of 4 m/s ($U^* = 58.82$), the absolute growth rates become nearly zero. The stabilization effect of velocity is

more significant at large electric fields. The result for the PIB Boger fluid is illustrated in Fig. 8. As is shown in the figure, the variation of the absolute growth rate with the velocity is generally the same as in the case of the PEO aqueous solution. Most significantly, absolute instability of the non-axisymmetric mode is depressed as the velocity of jet is increased, especially at large electric fields.

To better understand the role of the velocity, the absolute and convective instability transition boundary on the $U^* - \varpi$ plane is plotted in Figs. 9 and 10 for the PEO aqueous solution and the PIB Boger fluid, respectively. In the figures solid line denotes the boundary of the axisymmetric mode, below which is the absolute instability region of the mode and above which is its convective instability region; dashed line denotes the boundary of the first non-axisymmetric mode, below which is its absolute instability region and above which is its convective instability region. For both modes and both liquids, it can be seen that, at a fixed electric field, the instability of jet transits from absolute to convective when the velocity of jet is increased to a certain critical value. On the other hand, at a fixed velocity, the instability may change from convective to absolute when the electric field is increased up to some critical value. For the axisymmetric mode of the PEO aqueous solution, as is shown in Fig. 9, there exists a minimum velocity ($U^* \approx 54.5$ and $U \approx 3.8$ m/s), and when the velocity of the jet is smaller than this value, the jet is absolutely unstable no matter how large the electric field is. In Fig. 9 the narrow region between two boundary lines is absolute for the axisymmetric mode and convective for the non-axisymmetric mode, indicating that for the PEO aqueous solution the

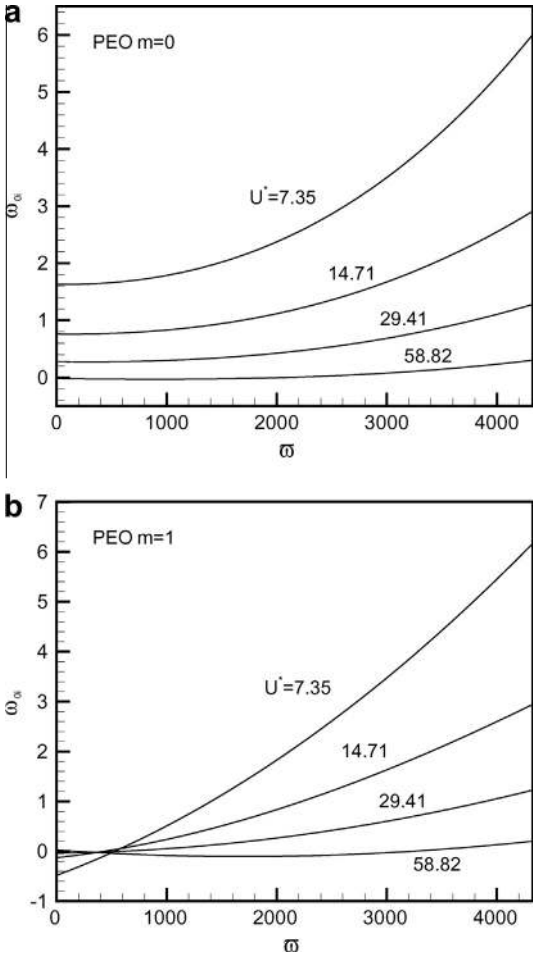

Fig. 7. Variation of the absolute growth rate ω_{0i} with the nondimensional velocity of jet U^* for (a) the axisymmetric mode $m = 0$ and (b) the non-axisymmetric mode $m = 1$ of the PEO aqueous solution.

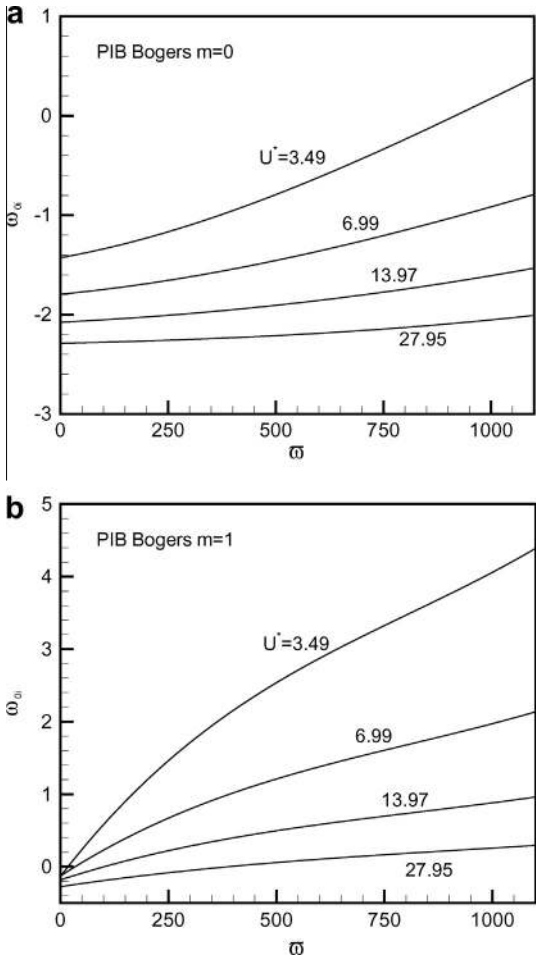

Fig. 8. Variation of the absolute growth rate ω_{0i} with the nondimensional velocity of jet U^* for (a) the axisymmetric mode $m = 0$ and (b) the non-axisymmetric mode $m = 1$ of the PIB Boger fluid.

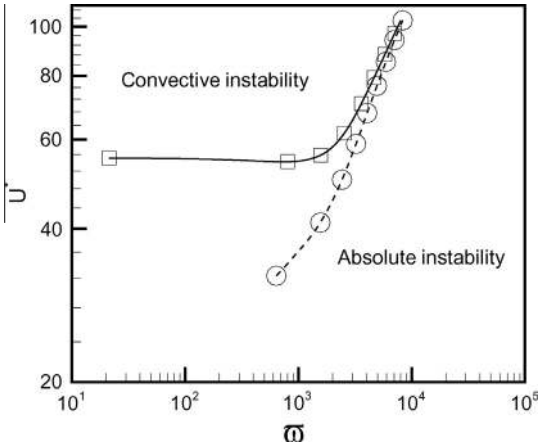

Fig. 9. The boundary between absolute and convective instability of the axisymmetric mode $m = 0$ (solid line) and the non-axisymmetric mode $m = 1$ (dashed line) of the PEO aqueous solution on the $U^* - \varpi$ plane.

axisymmetric mode is dominant over the non-axisymmetric mode. However, the predominance of the axisymmetric mode tends to disappear at large electric fields. In Fig. 10 the axisymmetric mode of the PIB Boger fluid is convectively unstable in the explored field except in a small region (below at the right) with large electric fields and small jet velocities. Between the two boundary lines there is a

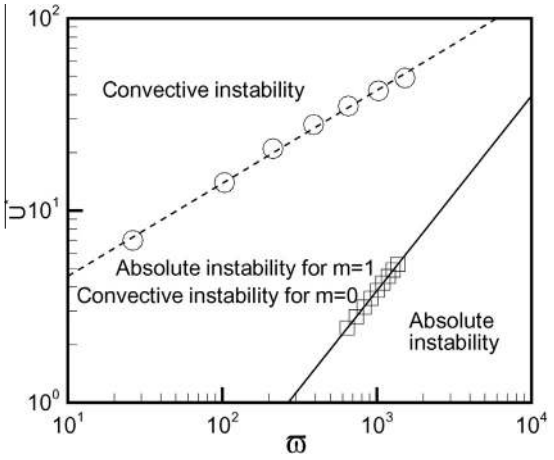

Fig. 10. The boundary between absolute and convective instability of the axisymmetric mode $m = 0$ (solid line) and the non-axisymmetric mode $m = 1$ (dashed line) of the PIB Boger fluid on the $U^* - \varpi$ plane.

wide region in which the axisymmetric mode is convectively unstable and the non-axisymmetric mode is absolutely unstable. In this region the non-axisymmetric mode is dominant. Above the dashed line both modes are convectively unstable.

Now the velocity of jet is fixed to 1 m/s and the radius of jet is varied between several values: 2.5 μm, 5 μm, 10 μm, 20 μm and 40 μm. Taking $R_c = \eta_0^2/\rho\gamma$ as a scale, we define a nondimensional jet radius $R^* = R/R_c$. The absolute and convective instability characteristic of the PEO aqueous solution and the PIB Boger fluid jets are demonstrated in Figs. 11 and 12, respectively, where the abscissa is the nondimensional electrostatic force ϖ. It is shown that the influence of the jet radius on the absolute growth rate of the axisymmetric mode of the PEO aqueous solution is non-monotonic. As the jet radius is decreased, the absolute growth rate is increased moderately at relatively small electric fields but is decreased to a great extent at relatively large electric fields. On the other hand, the absolute growth rate of the non-axisymmetric mode is decreased as the jet radius is decreased, especially at large electric fields. In the scope of present research both the axisymmetric and the non-axisymmetric modes are absolutely unstable. For the PIB Boger fluid, the absolute growth rate of the axisymmetric mode is decreased as the radius is decreased. This mode is convectively unstable except when the radius and the electric field are sufficiently large. For the non-axisymmetric mode the influence of jet radius is quite limited. With the absolute growth rate reduced slightly as the radius of jet is decreased, the non-axisymmetric mode remains in the absolute instability domain. Generally, although absolute instability cannot be eliminated by decreasing or increasing the radius of jet, it can be weakened to a certain extent in all the cases.

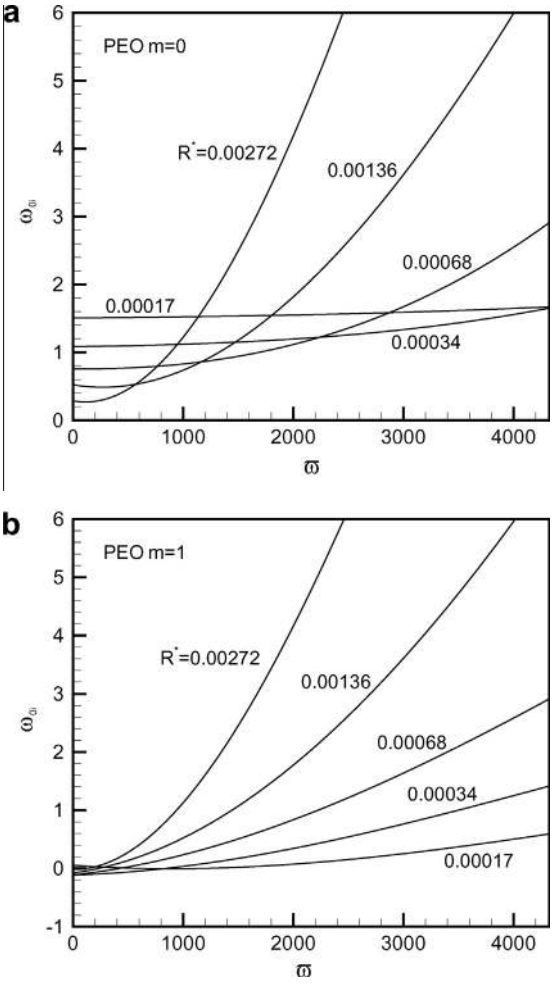

Fig. 11. Variation of the absolute growth rate ω_{0i} with the nondimensional radius of jet R^* for (a) the axisymmetric mode $m = 0$ and (b) the non-axisymmetric mode $m = 1$ of the PEO aqueous solution.

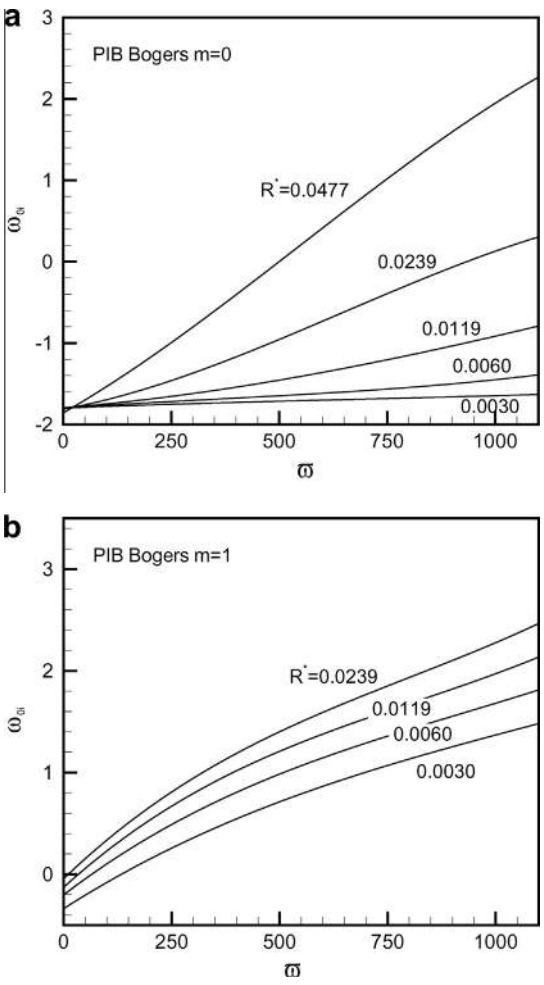

Fig. 12. Variation of the absolute growth rate ω_{0i} with the nondimensional radius of jet R^* for (a) the axisymmetric mode $m = 0$ and (b) the non-axisymmetric mode $m = 1$ of the PIB Boger fluid.

The absolute and convective instability transition boundary on the $R^* - \varpi$ plane is plotted in Figs. 13 and 14 for the PEO aqueous solution and the PIB Boger fluid, respectively, where solid line denotes the boundary of the axisymmetric mode and dashed line denotes the boundary of the first non-axisymmetric mode. In Fig. 13, the small region in the upper left corner confined by the solid line, which possesses large jet radii ($R^* > 0.011$ and $R > 160\ \mu m$) and small electric fields, is the convective instability domain of the axisymmetric mode of the PEO aqueous solution, and in the large region beyond it the axisymmetric mode is absolutely unstable. The transition boundary of the non-axisymmetric mode is like an asymptotic line in both the R^* and ϖ directions. The region up and to the right of the boundary is absolute instability for the non-axisymmetric mode, while in the region below and to the left of the line the mode is stable or convectively unstable. It should be noted that in this below left region the axisymmetric mode is dominant since it is absolutely unstable. In Fig. 14 both the transition boundary of the axisymmetric mode and that of the non-axisymmetric mode of the PIB Boger fluid possess asymptotic characteristic. At a fixed jet radius, the instability of the modes may transit from convective to absolute when the electric field exceeds a critical value. On the other hand, at a fixed electric field, the instability may transit from convective to absolute when the radius of the jet exceeds a critical value. Note that the stable or convectively unstable region of the non-axisymmetric mode is quite small. That is, at the jet velocity considered here ($U = 1$ m/s), the absolute instability of the non-axisymmetric mode of the PIB Boger fluid is easily induced by the electric field. In addition, in the region between two boundary lines where the axisymmetric mode is convectively unstable and the non-axisymmetric mode is absolutely unstable, the non-axisymmetric mode is dominant.

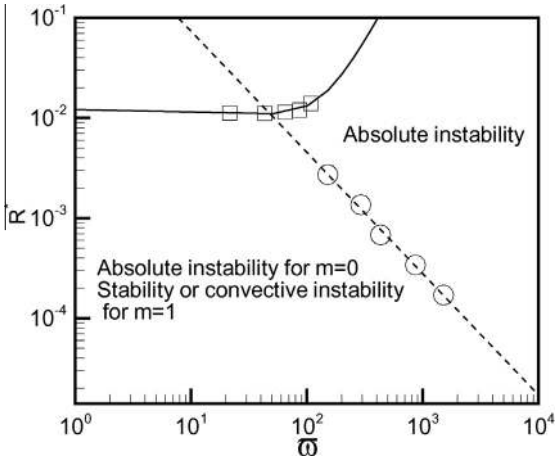

Fig. 13. The boundary between absolute and convective instability of the axisymmetric mode $m = 0$ (solid line) and the non-axisymmetric mode $m = 1$ (dashed line) of the PEO aqueous solution on the $R^* - \varpi$ plane.

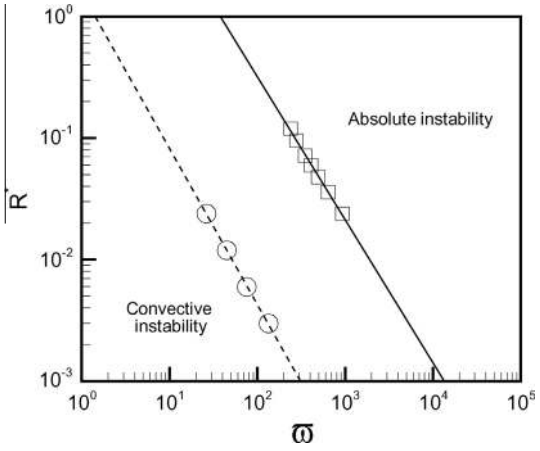

Fig. 14. The boundary between absolute and convective instability of the axisymmetric mode $m = 0$ (solid line) and the non-axisymmetric mode $m = 1$ (dashed line) of the PIB Boger fluid on the $R^* - \varpi$ plane.

4. Conclusion

In this work we explore the absolute and convective instability of a charged viscoelastic liquid jet through a linear model built for three-dimensional infinitesimal disturbances, aiming to the establishment of a general, complete knowledge and predictive framework for the benefit of industrial processes.

Consistently with previous studies for Newtonian liquids, it is found that normal electric field may induce and augment the absolute instability of both the axisymmetric and non-axisymmetric modes of a viscoelastic jet. Moreover, the destabilization effect of electric field on the non-axisymmetric mode is more significant. Elasticity may also induce and enhance absolute instability of unstable modes, especially the axisymmetric one. The way to suppress absolute instability is explored. It is found that absolute instability of both the axisymmetric and non-axisymmetric modes may be weakened through increasing the velocity of jet and adjusting (in most situations decreasing) the jet radius.

According to the calculation, an electrified viscoelastic jet seems prone to become absolutely unstable, particularly when it is subjected to non-axisymmetric disturbances. However, experiments show that a viscoelastic jet can be well controlled under a globally stable state. This discrepancy between theory and experiments might be explained from several aspects. First, in electrohydrodynamically generated jets, there usually exists an externally applied tangential electric field (not considered in this work) which might suppress absolute instability and benefit convective instability. Second, absolute and convective instability only reflects local instability characteristics, and absolute instability does not necessarily lead to global instability, especially when the radius of the jet changes along the axial coordinate. Third, non-linear effects may be of paramount importance in electrified viscoelastic jets, where the role of elasticity as well as the other parameters might be quite different from the linear case. The investigation of these issues remains of particular interest for the future.

Acknowledgements

The work is funded by the National Natural Science Foundation of China (Projects No. 11272307 and No. 11002139) and the Fundamental Research Funds for the Central Universities. Dr. Li thanks for the support of Juan de la Cierva Program in Spain.

Appendix A. Expressions of the matrices in the eigenvalue problem (20)

$$[D] = \begin{bmatrix} [0]_{1\times(4N+6)} & & \\ D_{2a} & [0]_{(N-1)\times(3N+5)} & \\ [0]_{2\times(4N+6)} & & \\ [0]_{(N-1)\times(N+1)} & D_{4b} & [0]_{(N-1)\times(2N+4)} \\ [0]_{2\times(4N+6)} & & \\ [0]_{(N-1)\times(2N+2)} & D_{6b} & [0]_{(N-1)\times(N+3)} \\ [0]_{(N+4)\times(4N+6)} & & \end{bmatrix},$$

where [0] denotes zero matrix and the subscript denotes its size, $D_{2a} = D_e \cdot [T_n(y_j)]$, a matrix of size $(N-1)\times(N+1)$, row: $j = 1, \ldots, N-1$; column: $n = 0, 1, \ldots, N$; in expansion form

$$D_{2a} = D_e \cdot \begin{bmatrix} T_0(y_1) & T_1(y_1) & \cdots & T_N(y_1) \\ T_0(y_2) & T_1(y_2) & \cdots & T_N(y_2) \\ \vdots & \vdots & \ddots & \vdots \\ T_0(y_{N-1}) & T_1(y_{N-1}) & \cdots & T_N(y_{N-1}) \end{bmatrix}, \text{ and } D_{4b} = D_{6b} = D_{2a}.$$

$$[C] = \begin{bmatrix} C_{1x} & & & & & \\ C_{2a} & C_{2b} & [0]_{(N-1)\times(N+1)} & C_{2d} & [0]_{(N-1)\times 2} & \\ C_{3a} & [0]_{1\times(2N+2)} & C_{3c} & C_{3d} & C_{3e} & \\ C_{4x} & & & & & \\ C_{5a} & C_{5b} & [0]_{(N-1)\times(N+1)} & C_{5d} & [0]_{(N-1)\times 2} & \\ C_{6a} & C_{6b} & [0]_{1\times(2N+2)} & C_{6d} & C_{6e} & \\ C_{7x} & & & & & \\ [0]_{(N-1)\times(2N+2)} & C_{8b} & C_{8c} & [0]_{(N-1)\times 2} & & \\ C_{9a} & [0]_{1\times(N+1)} & C_{9c} & [0]_{1\times(N+1)} & C_{9e} & C_{9f} \\ C_{10x} & & & & & \\ C_{11a} & C_{11b} & C_{11c} & [0]_{N\times(N+3)} & & \\ [0]_{1\times(4N+5)} & 1 & & & & \\ [0]_{1\times(4N+4)} & 1 & 0 & & & \end{bmatrix}$$

where

$$C_{1x} = \begin{cases} [T_0(-1) \;\; T_1(-1) \;\; \cdots \;\; T_N(-1) \;\; [0]_{1\times(3N+5)}] & \text{if } m = 0 \\ [T_0(-1) \;\; \cdots \;\; T_N(-1) \;\; iT_0(-1) \;\; \cdots \;\; iT_N(-1) \;\; [0]_{1\times(2N+4)}] & \text{if } m = 1 \end{cases};$$

$$C_{2a} = \left[-\frac{\lambda^* k}{R_e}\left(4T_n''(y_j) + \frac{4}{1+y_j}T_n'(y_j) - \left(\frac{4(m^2+1)}{(1+y_j)^2} + k^2 + \frac{R_e(1+2ikD_e)}{\lambda^*} \right) T_n(y_j) \right) \right],$$

$$C_{2b} = \left[-\frac{8m\lambda^*}{R_e(1+y_j)^2} T_n(y_j) \right], \quad C_{2d} = [2iD_e T_n'(y_j)],$$

C_{2a}, C_{2b}, and C_{2d} are matrices of size $(N-1)\times(N+1)$, row: $j = 1, \ldots, N-1$; column: $n = 0, 1, \ldots, N$;

$$C_{3a} = \left[-\frac{4i\lambda^*}{R_e} T_n'(1) \right], \quad C_{3c} = [iD_e T_n(1)],$$

C_{3a} and C_{3c} are matrices of size $1\times(N+1)$, column: $n = 0, 1, \ldots, N$;

$$C_{3d} = iD_e E_u \left(1 - \frac{\varepsilon_r}{\zeta} \right), \quad C_{3e} = iD_e \left(\frac{1 - m^2 - k^2}{W_e} - E_u \frac{\varepsilon_r \xi}{\zeta} \right);$$

$$C_{4x} = \begin{cases} [[0]_{1\times(N+1)} \;\; T_0(-1) \;\; T_1(-1) \;\; \cdots \;\; T_N(-1) \;\; [0]_{1\times(2N+4)}] & \text{if } m = 0 \\ [2T_0'(-1) \;\; \cdots \;\; 2T_N'(-1) \;\; iT_0'(-1) \;\; \cdots \;\; iT_N'(-1) \;\; [0]_{1\times(2N+4)}] & \text{if } m = 1 \end{cases};$$

$$C_{5a} = -C_{2b}, \quad C_{5b} = C_{2a}, \quad C_{5d} = \left[-\frac{2mD_e}{1+y_j} T_n(y_j) \right],$$

C_{5a}, C_{5b} and C_{5d} are matrices of size $(N-1)\times(N+1)$, row: $j = 1, \ldots, N-1$; column: $n = 0, 1, \ldots, N$;

$$C_{6a} = \left[\frac{i\lambda^*}{R_e} imT_n(1) \right], \quad C_{6b} = \left[\frac{i\lambda^*}{R_e} (2'T_n(1) - T_n(1)) \right],$$

C_{6a} and C_{6b} are matrices of size $1\times(N+1)$, column: $n = 0, 1, \ldots, N$;

$$C_{6d} = iD_e \frac{imE_u}{k\zeta} \frac{I_m(k)}{I_m'(k)}, \quad C_{6e} = C_{6d}\xi;$$

$$C_{7x} = \begin{cases} \left[[0]_{1\times(2N+2)} \;\; T_0'(-1) \;\; T_1'(-1) \;\; \cdots \;\; T_N'(-1) \;\; [0]_{1\times(N+3)} \right] & \text{if } m = 0 \\ [\,[0]_{1\times(2N+2)} \;\; T_0(-1) \;\; T_1(-1) \;\; \cdots \;\; T_N(-1) \;\; [0]_{1\times(N+3)}\,] & \text{if } m = 1 \end{cases};$$

$$C_{8b} = \left[-\frac{i\lambda^*}{R_e}\left(4T_n''(y_j) + \frac{4}{1+y_j}T_n'(y_j) - \left(\frac{4m^2}{(1+y_j)^2} + k^2 + \frac{R_e(1+2ikD_e)}{\lambda^*} \right) T_n(y_j) \right) \right],$$

$$C_{8c} = [-kD_e T_n(y_j)],$$

C_{8b} and C_{8c} are matrices of size $(N-1)\times(N+1)$, row: $j = 1, \ldots, N-1$; column: $n = 0, 1, \ldots, N$;

$$C_{9a} = \left[\frac{i\lambda^*}{R_e} ikT_n(1) \right], \quad C_{9c} = \left[\frac{i\lambda^*}{R_e} 2T_n'(1) \right],$$

C_{9a} and C_{9c} are matrices of size $1\times(N+1)$, column: $n = 0, 1, \ldots, N$;

$C_{9e} = iD_e \frac{iE_u}{\zeta} \frac{I_m(k)}{I_m'(k)}$ and $C_{9f} = C_{9e}\xi$;

$$C_{10x} = \begin{cases} \left[[0]_{1\times(3N+3)} \;\; T_0'(-1) \;\; T_1'(-1) \;\; \cdots \;\; T_N'(-1) \;\; [0]_{1\times 2} \right] & \text{if } m - 0 \\ [\,[0]_{1\times(3N+3)} \;\; T_0(-1) \;\; T_1(-1) \;\; \cdots \;\; T_N(-1) \;\; [0]_{1\times 2}\,] & \text{if } m = 1 \end{cases};$$

$$C_{11a} = \left[2T_n'(y_j) + \frac{2}{1+y_j} T_n(y_j) \right], \quad C_{11b} = \left[\frac{2im}{1+y_j} T_n(y_j) \right], \quad C_{11c} = [ikT_n(y_j)],$$

C_{11a}, C_{11b} and C_{11c} are matrices of size $N\times(N+1)$, row: $j = 0, \ldots, N-1$; column: $n = 0,1, \ldots, N$.

$$[B] = \begin{bmatrix} B_{1x} & & & & & \\ B_{2a} & B_{2b} & [0]_{(N-1)\times(N+1)} & B_{2d} & [0]_{(N-1)\times 2} & \\ B_{3a} & [0]_{1\times(2N+2)} & B_{3c} & B_{3d} & B_{3e} & \\ B_{4x} & & & & & \\ B_{5a} & B_{5b} & [0]_{(N-1)\times(N+1)} & B_{5d} & [0]_{(N-1)\times 2} & \\ B_{6a} & B_{6b} & [0]_{1\times(2N+2)} & B_{6d} & B_{6e} & \\ B_{7x} & & & & & \\ [0]_{(N-1)\times(2N+2)} & B_{8b} & B_{8c} & [0]_{(N-1)\times 2} & & \\ B_{9a} & [0]_{1\times(N+1)} & B_{9c} & [0]_{1\times(N+1)} & B_{9e} & B_{9f} \\ B_{10x} & & & & & \\ B_{11a} & B_{11b} & B_{11c} & [0]_{N\times(N+3)} & & \\ B_{12x} & & & & & \\ B_{13x} & & & & & \end{bmatrix}$$

where

$$B_{1x} = C_{1x} \cdot er;$$

$$B_{2a} = \left[-\frac{1+i\lambda^* k}{R_e}\left(4T_n''(y_j) + \frac{4}{1+y_j}T_n'(y_j) - \left(\frac{4(m^2+1)}{(1+y_j)^2} + k^2 + \frac{R_e(ik - D_e k^2)}{1+i\lambda^* k} \right) T_n(y_j) \right) \right],$$

$$B_{2b} = \left[\frac{8im(1+i\lambda^* k)}{R_e(1+y_j)^2} T_n(y_j) \right], \quad B_{2d} = [2(1+ikD_e)T_n'(y_j)],$$

B_{2a}, B_{2b}, and B_{2d} are matrices of size $(N-1)\times(N+1)$, row: $j = 1, \ldots, N-1$; column: $n = 0, 1, \ldots, N$;

$$B_{3a} = \left[-\frac{4(1+i\lambda^* k)}{R_e} T_n'(1) \right], \quad B_{3c} = [(1+ikD_e)T_n(1)],$$

B_{3a} and B_{3c} are matrices of size $1\times(N+1)$, column: $n = 0, 1, \ldots, N$;

$$B_{3d} = (1+ikD_e)E_u \left(1 - \frac{\varepsilon_r}{\zeta} \right), \quad B_{3e} = (1+ikD_e) \left(\frac{1 - m^2 - k^2}{W_e} - E_u \frac{\varepsilon_r \xi}{\zeta} \right);$$

$$B_{4x} = C_{4x} \cdot er;$$

$$B_{5a} = -B_{2b}, \quad B_{5b} = B_{2a}, \quad B_{5d} = \left[\frac{2im}{1+y_j} (1+ikD_e) T_n(y_j) \right],$$

matrices of size $(N-1)\times(N+1)$, row: $j = 1, \ldots, N-1$; column: $n = 0, 1, \ldots, N$;

$$B_{6a} = \left[\frac{1+i\lambda^* k}{R_e} imT_n(1) \right], \quad B_{6b} = \left[\frac{1+i\lambda^* k}{R_e} (2'T_n(1) - T_n(1)) \right],$$

matrices of size $1 \times (N+1)$, column: $n = 0, 1, \ldots, N$;

$$B_{6d} = (1 + ikD_e)\frac{imE_u}{k\zeta}\frac{I_m(k)}{I'_m(k)} \text{ and } B_{6e} = B_{6d}\xi;$$

$$B_{7x} = C_{7x} \cdot er;$$

$$B_{8b} = \left[-\frac{1+i\lambda^* k}{R_e}\left(4T''_n(y_j) + \frac{4}{1+y_j}T'_n(y_j) - \left(\frac{4m^2}{(1+y_j)^2} + k^2 + \frac{R_e(ik - D_e k^2)}{1+i\lambda^* k}\right)T_n(y_j)\right)\right],$$

$$B_{8c} = [(ik - D_e k^2)T_n(y_j)],$$

B_{8b} and B_{8c} are matrices of size $(N-1) \times (N+1)$, row: $j = 1, \ldots, N-1$; column: $n = 0, 1, \ldots, N$;

$$B_{9a} = \left[\frac{1+i\lambda^* k}{R_e}ikT_n(1)\right], \quad B_{9c} = \left[\frac{1+i\lambda^* k}{R_e}2T'_n(1)\right],$$

matrices of size $1 \times (N+1)$, column: $n = 0, 1, \ldots, N$;

$$B_{9e} = (1 + ikD_e)\frac{iE_u}{\zeta}\frac{I_m(k)}{I'_m(k)} \text{ and } B_{9f} = B_{9e}\xi;$$

$$B_{10x} = C_{10x} \cdot er;$$

$$B_{11a} = C_{11a} \cdot er, \quad B_{11b} = C_{11b} \cdot er, \quad B_{11c} = C_{11c} \cdot er;$$

$$B_{12x} = \begin{bmatrix} iT_0(1) & iT_1(1) & \cdots & iT_N(1) & [0]_{1\times(3N+4)} & k \end{bmatrix};$$

$$B_{13x} = \left[\begin{array}{cccccc} 2iT'_0(1) & 2iT'_1(1) & \cdots & 2iT'_N(1) & [0]_{1\times(3N+3)} & k - \frac{i\tau_e e_r}{\zeta} \end{array} \quad -\frac{i\tau_e e_r \xi}{\zeta}\right],$$

and er is an arbitrary complex number unequal to unity.

References

[1] D.H. Reneker, A.L. Yarin, Electrospinning jets and polymer nanofibers, Polymer 49 (2008) 2387–2425.
[2] O. Regev, S. Vandebril, E. Zussman, C. Clasen, The role of interfacial viscoelasticity in the stabilization of an electrospun jet, Polymer 51 (2010) 2611–2620.
[3] H. Moghadam, M. Samimi, A. Samimi, M. Khorram, Electrospray modeling of highly viscous and non-Newtonian liquids, J. Appl. Polym. Sci. 118 (2010) 1288–1296.
[4] M. Pakravan, M.-C. Heuzey, A. Ajji, A fundamental study of chitosan/PEO electrospinning, Polymer 52 (2011) 4813–4824.
[5] D.H. Reneker, A.L. Yarin, H. Fong, S. Koombhongse, Bending instability of electrically charged liquid jets of polymer solutions in electrospinning, J. Appl. Phys. 87 (2000) 4531–4547.
[6] A.L. Yarin, S. Koombhongse, D.H. Reneker, Bending instability in electrospinning of nanofibers, J. Appl. Phys. 89 (2001) 3018–3026.
[7] G. Brenn, Z. Liu, F. Durst, Linear analysis of the temporal instability of axisymmetric non-Newtonian liquid jets, Int. J. Multiphase Flow 26 (2000) 1621–1644.
[8] Z. Liu, Z. Liu, Linear analysis of three-dimensional instability of non-Newtonian liquid jets, J. Fluid Mech. 559 (2006) 451–459.
[9] Z. Liu, Z. Liu, Instability of a viscoelastic liquid jet with axisymmetric and asymmetric disturbances, Int. J. Multiph. Flow 34 (2008) 42–60.
[10] C.P. Carroll, Y.L. Joo, Axisymmetric instabilities of electrically driven viscoelastic jets, J. Non-Newtonian Fluid Mech. 153 (2008) 130–148.
[11] C.P. Carroll, Y.L. Joo, Axisymmetric instabilities in electrospinning of highly conducting, viscoelastic polymer solutions, Phys. Fluids 21 (2009) 103101.
[12] J.M. Montanero, A.M. Gañán-Calvo, Viscoelastic effects on the jetting-dripping transition in co-flowing capillary jets, J. Fluid Mech. 610 (2008) 249–260.
[13] F. Li, X.-Y. Yin, X.-Z. Yin, Axisymmetric and non-axisymmetric instability of an electrically charged viscoelastic liquid jet, J. Non-Newtonian Fluid Mech. 166 (2011) 1024–1032.
[14] A.-C. Ruo, F. Chen, C.-A. Chung, M.-H. Chang, Three-dimensional response of unrelaxed tension to instability of viscoelastic jets, J. Fluid Mech. 682 (2011) 558–576.
[15] A.-C. Ruo, K.-H. Chen, M.-H. Chang, F. Chen, Instability of a charged non-Newtonian liquid jet, Phys. Rev. E 85 (2012) 016306.
[16] Z.-M. Huang, Y.-Z. Zhang, M. Kotaki, S. Ramakrishna, A review on polymer nanofibers by electrospinning and their applications in nanocomposites, Compos. Sci. Technol. 63 (15) (2003) 2223–2253.
[17] J.B. Fenn, M. Mann, C.K. Meng, S.F. Wong, Electrospray ionization-principles and practice, Mass Spectrom. Rev. 9 (1990) 37–70.
[18] A. Greiner, J.H. Wendorff, Electrospinning: a fascinating method for the preparation of ultrathin fibers, Angew. Chem. Int. Ed. 46 (2007) 5670–5703.
[19] M.M. Hohman, M. Shin, G. Rutledge, M.P. Brenner, Electrospinning and electrically forced jets. I. Stability theory, Phys. Fluids 13 (8) (2001) 2201–2220.
[20] S.J. Gaskell, Electrospray: principles and practice, J. Mass Spectrom. 32 (7) (1997) 677–688.
[21] T. Si, G.-B. Li, X.-X. Chen, R.-J. Tian, X.-Z. Yin, Experimental investigation on flow modes of electrospinning, Acta Mech. Sin. 28 (3) (2012) 644–652.
[22] Y.M. Shin, M.M. Hohman, M.P. Brenner, G.C. Rutledge, Experimental characterization of electrospinning: the electrically forced jet and instabilities, Polymer 42 (2001) 9955–9967.
[23] S.A. Theron, E. Zussman, A.L. Yarin, Experimental investigation of the governing parameters in the electrospinning of polymer solutions, Polymer 45 (6) (2004) 2017–2030.
[24] J.M. López-Herrera, A.M. Gañán-Calvo, M.A. Herrada, Absolute to convective instability transition in charged liquid jets, Phys. Fluids 22 (2010) 062002.
[25] F. Li, A.M. Gañán-Calvo, J.M. López-Herrera, Absolute-convective instability transition of low permittivity, low conductivity charged viscous liquid jets under axial electric fields, Phys. Fluids 236 (2011) 094108.
[26] M.A. Herrada, J.M. Montanero, C. Ferrera, A.M. Gañán-Calvo, Analysis of the dripping-jetting transition in compound capillary jets, J. Fluid Mech. 649 (2010) 523–536.
[27] E.J. Vega, J.M. Montanero, M.A. Herrada, A.M. Gañán-Calvo, Global and local instability of flow focusing: the influence of the geometry, Phys. Fluids 22 (2010) 064105.
[28] J.M. Montanero, N. Rebollo-Muñoz, M.A. Herrada, A.M. Gañán-Calvo, Global stability of the focusing effect of fluid jet flows, Phys. Rev. E 83 (2011) 036309.
[29] A.J. Acero, C. Ferrera, J.M. Montanero, A.M. Gañán-Calvo, Focusing liquid microjets with nozzles, J. Micromech. Microeng. 22 (2012) 065011.
[30] S.P. Lin, Breakup of Liquid Sheets and Jets, Cambridge University Press, 2003.
[31] T. Si, F. Li, X.-Y. Yin, X.-Z. Yin, Modes in flow focusing and instability of coaxial liquid-gas jets, J. Fluid Mech. 629 (2009) 1–23.
[32] C. Clasen, J. Bico, V.M. Entov, G.H. McKinley, 'Gobbling drops': the jetting-dripping transition in flows of polymer solutions, J. Fluid Mech. 636 (2009) 5–40.
[33] D.F. James, Boger fluids, Annu. Rev. Fluid Mech. 41 (2009) 129–142.
[34] D.A. Saville, Electrohydrodynamics: the Taylor–Melcher leaky dielectric model, Annu. Rev. Fluid Mech. 29 (1997) 27–64.
[35] P.J. Schmid, D.S. Henningson, Stability and Transition in Shear Flows, Springer, 2001.